Reversion Scheme for Droplet Parameters with Rainbow Refractometry based on Debye Theory

Feihu Song, Zhibiao Yao, Chuanlong Xu *, Shimin Wang

*Corresponding author: Tel.: +86 025 83794395; Email: chuanlongxu@seu.edu.cn

Thermal Energy Engineering Research Institute, Southeast University, Nanjing, 210096, China.

Abstract: Rainbow refractometry is a non-intrusive technology for determining the refractive index and diameter of droplet simultaneously. Most of the present schemes for the refractive index and diameter of droplet are based on empirical formulas with Airy theory. However, the anti-noise capability and the generality of the empirical method are weak. In the paper, an objective function was designed to quantify the deviation between the low frequency component of the captured rainbow and the simulated rainbow with Debye (p=2) theory. Further, a novel inversion scheme for single droplet based on Debye (p=2) theory and the objective function was proposed. Experiments were carried out to evaluate the performance of the scheme. Results indicate that the relative error of the radius is less than 8%, the absolute error of the refractive index is better than 5×10^{-4}.

Keywords: Rainbow refractometry, Refractive index, Diameter, Debye theory

1 Introduction

The parameters (diameter, temperature, concentration .etc) of the droplet play an important role in the quality of many industrial processes such as combustion, cooling, drying and humidifying. The real-time and accurate measurement of the parameters is helpful to improve their production efficiency, optimize product quality and control pollutant emission. Optical technology is widely used for droplet measurement at present because of its non-invasion, high precision, high resolution in time and space and real-time performance. Rainbow refractometry is one of light scattering detection technologies, which can measure the diameter and refractive index simultaneously with the intensity distribution in specific angular range. As a result the parameters (temperature, concentration .etc) related to the refractive index can be calculated by certain functions indirectly [1-5]. The scattering angles of the rays experiencing one internal reflection in the droplet have a minimum value named the first-order geometric predicted rainbow angle. Rainbow refractometry can be used to detect the refractive index and the diameter of the droplet through the intensity distribution near the first-order geometric predicted rainbow angle. Compared with the scattering light in other angular ranges, the first-order rainbow has the following advantages:

(1) Its structure is stable. Limited distortions of the droplet parameter do not destroy the rainbow, but change its position only.

(2) Its resolution is high. The first-order rainbow changes obviously when the refractive index and the diameter of the droplets changes a little.

(3) Its scattering intensity is big. The intensity of the ray becomes weaker as the increase of internal reflections in the droplet.

(4) Its information content is rich. Fluctuations of various frequencies can be seen from the first-order rainbow.

(5) The optical path of the ray experiencing one internal reflection is so simple that other mature theory (such as geometric optics) can be combined.

Measurement technologies based on the first-order rainbow are investigated and applied widely due to its unique advantages. Roth placed two CCD cameras in the forward area around 30° and the background area around 140° to capture the scattering intensity.

Then the refractive index was determined by the forward scattering intensity and the diameter was determined by the background scattering intensity according to the Airy theory [2-4]. Van Beeck placed only one CCD camera in the background area to simplify the measurement system. Then refractive index was determined by the location of the peak intensity and diameter was determined by the supernumerary bows [5]. Wu presented an empirical formula for the droplet diameter and refractive index based on the supernumerary bows and the ripple bows [6]. However, most of the present methods are based on empirical formula. Their accuracy is low and the anti-noise capability is low on the premise that the diameter and refractive index are changed in a broad range. Additionally, measurement error transfer occurs due to the coupling among the parameters [7].

To solve the problems above, the paper presents an improved scheme for the parameters of singe droplet based on Debye theory. The calculation results of the empirical formula are taken as the initial parameters. Then the intensity distribution of the first rainbow is simulated by Debye theory (p=2) according to the initial parameters. An objective function is designed to quantify the deviation between the low frequency component of the captured rainbow and the simulated rainbow. Finally the initial parameters are optimized continuously for the purpose of decreasing the objective function value. Experiments are also carried out to investigate the performance of the reversion scheme.

2 Measurement theory

2.1 Thoery of rainbow refractometry

If a homogeneous droplet is illuminated by a monochrome laser, the first-order rainbow can be produced by the rays experiencing several internal reflections, the externally reflected rays on the droplet and surface wave. Fig.1 shows the optical path of the ray experiencing one internal reflection at the section of the droplet. As shown in Fig.1, the scattering light is denoted by I_{out}, the incident light by I_{in}, the incident angle by α, the refraction angle by β, the scattering angle by θ , the radius of the section by R and the ratio of the refractive index of the droplet and one of the surrounding medium by m .

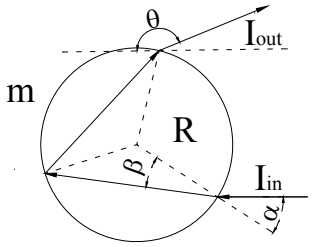

Fig.1 Optical path at the section of the column

According to the geometrical optics and Fig. 1, equation (1) can be obtained

$$\theta = 2\pi - 4\beta + 2\alpha = 2\pi - 4\sin^{-1}(\frac{\sin\alpha}{m}) + 2\alpha \quad (1)$$

From equation (1), there is a minimum scattering angle defined as the geometrical predicted rainbow angle θ_{rg}, where the scattering light is dense. θ_{rg} can be calculated as

$$\theta_{rg} = 2\pi - 4\sin^{-1}\sqrt{\frac{4-m^2}{3m^2}} + 2\sin^{-1}\sqrt{\frac{4-m^2}{3}} \quad (2)$$

From equation (2), the refractive index m can be determined by measuring θ_{rg}. Actually the angular location of the peak intensity deviates from the geometrical predicted rainbow angle, so θ_{rg} cannot be directly detected.

Geometric optics can analyze each ray independently, and yet the interference among all the rays cannot be depicted. The Airy theory can compute the intensities around the geometrical predicted rainbow angle through the use of the Fresnel theory combined with the rainbow method [8-9]. The Lorenz-Mie theory is used to accurately compute the scattering intensity of an illuminated sphere after the birth of Maxwell electromagnetic theory [10]. Fig.2 illustrates the simulated first-order rainbow based on Mie theory and the Airy theory respectively. The droplet radius is 250 μm, the refractive index is 1.3326 and the wavelength is 532nm. From Fig.2, it can be

seen that the location of each supernumerary bow in a certain curve deviates from the corresponding maximum in the other curve. The frequency spectrums corresponding to Fig.2 are shown in Fig.3. It can be seen from the curve simulated by Mie theory that there are several obvious frequency peaks, mainly including the frequency of supernumerary bows, frequency of ripple bows superimposed on the supernumerary bows and frequency of higher frequency structure caused by the interference between the diffraction rays and reflection rays (internal and external). On the contrary, the Airy theory can only simulate the supernumerary bows of the rainbow and the frequency of the supernumerary bows is smaller than that simulated by Mie theory. The rainbow pattern will be moved and stretched when the parameters of the droplet change. Therefore, the droplet parameters can be determined by the intensity distribution captured by a CCD camera.

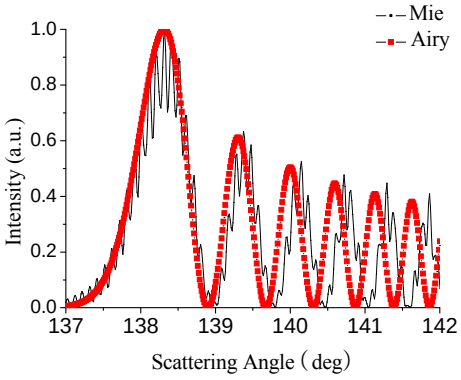

Fig.2 First-order rainbow simulated by Mie theory and the Airy theory (m=1.3326, R=250 μm, λ=532nm)

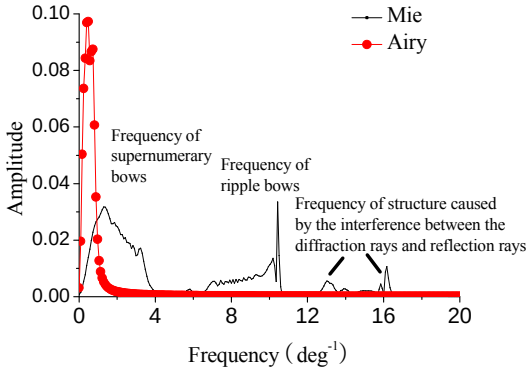

Fig.3 Frequency spectrum of rainbow corresponding to Fig. 2

2.2 Scattering analysis base on Debye theory

Mie coefficient can be decomposed by Debye theory. Consequently the contribution of each ray can be obtained [11]. Debye coefficient is expressed as:

$$\left.\begin{matrix} a_n \\ b_n \end{matrix}\right\} = \frac{1}{2}[1 - R_n^{212} - \sum_{p=1}^{\infty} T_n^{21}(R_n^{121})^{p-1} T_n^{12}] \quad (3)$$

where n is the index of the infinite series, R_n^{212} and R_n^{121} are reflection coefficients, T_n^{21} and T_n^{12} are transmission coefficients, the first term on the right of equation (3) corresponds to the diffraction rays, the second term corresponds to the external reflection rays and the third term corresponds to the rays experiencing p-1 internal reflections. Mie coefficients can be obtained by adding each term on the right of the equal sign in equation (3) when p varies from 1 to a number large enough. The supernumerary bows of the first-order rainbow is formed by the interference of the p=2 rays, so the Debye coefficient is $T_n^{21}R_n^{121}T_n^{12}$. Fig.4 illustrates the low frequency component of the rainbow simulated by Mie theory and the supernumerary bows simulated by Debye theory (p=2), respectively. The cutoff frequency of the low frequency component of the rainbow simulated by Mie theory is its supernumerary frequency. So is the cutoff frequency in the text below. From Fig.4, it is obvious that the angular locations of corresponding maxima in the three curves are almost equal.

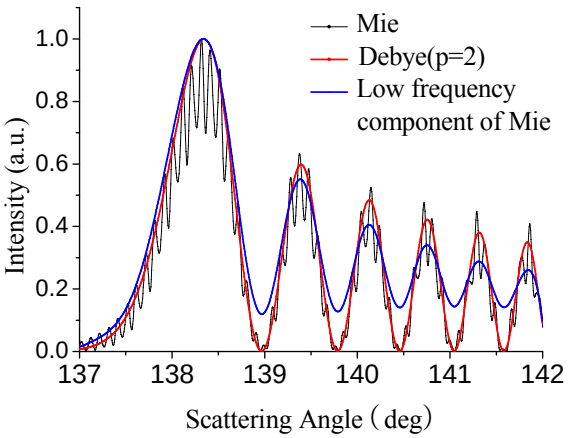

Fig.4 Comparison of low frequency component of the rainbow simulated by Mie theory and by Debye theory (p=2) (m=1.3326, R=250 μm, λ=532nm)

2.3 Objective function

The predicted parameters are considered to be the true values of the droplet if the intensity distribution simulated by Mie theory according to the predicted parameters coincides with the captured rainbow well. To quantify the deviation between the captured light intensity and the simulated rainbow, an objective function is designed.

$$f(m,R)=\sum_{k=1}^{n}[I_{mea}(k)-I_{sim}(k)]^2 \quad (4)$$

where f is objective function value, I_{mea} is the rainbow captured by the CCD camera, I_{sim} is the simulated rainbow, k is the serial number of the discrete angular positions selected and n is the total number of the discrete points. The objective function is based on Mie theory if I_{sim} in equation (4) is simulated by Mie theory. Otherwise it is based on Debye theory if I_{sim} is simulated by Debye theory (p=2) and I_{mea} is the low frequency component of the captured rainbow. There are several maxima in the rainbow simulated by Mie theory due to the high frequency component. So the change in the value of the objective function based on Mie theory is complex. On the contrary, the rainbow simulated by Debye theory has simpler structure. Considering the good coincidence between curves simulated by the two theories, the objective function based on Debye theory is used to ensure the efficiency and accuracy of the scheme. Discrete points used in the objective function are expressed as.

$$\theta(k)=(\theta_{r1}-\theta_{l1})/14+\theta_{l1},k=0,2,\ldots,14 \quad (5)$$

$$\theta(k)=(\theta_{r2}-\theta_{l2})/8+\theta_{l2},k=0,2,\ldots,8 \quad (6)$$

Equation (5) describes the points in the first supernumerary bow, and equation (6) describes the points in the second supernumerary bow. At θ_{l1} the intensity firstly equals to 40% of the peak amplitude of the first supernumerary bow when searching leftward from the peak. θ_{r1}, θ_{l2} and θ_{r2} have the similar definitions. The four angles are schematically shown in Fig.5. Three main reasons should be considered when selecting the discrete points:

(1) The computation of Mie theory and Debye theory is complex. So that only a few discrete points are used is helpful to induce time-consumption.

(2) Concerning the first supernumerary bow, the curve simulated by Debye theory (p=2) deviates form the low frequency component curve slightly, as is shown in Fig.4, while the second supernumerary bow has the better coincidence.

(3) The first two supernumerary bows have bigger signal to noise ratio due to their bigger amplitude.

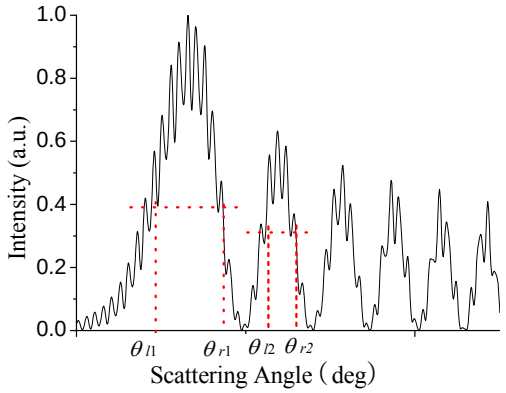

Fig.5 Schematic diagram of θ_{l1}, θ_{l2}, θ_{r1} and θ_{r2}

3 Reversion scheme

Reversion scheme is put forward to determine the refractive index and radius based on Mie theory, Debye theory and the objective function. Reversion scheme consists of three steps: first the initial radius and refractive index of the droplet are determined by an empirical formula; then the initial values are optimized continuously by decreasing the value of the objective function based on Debye theory; finally the final result is determined by further searching parameter-pairs around the optimization result based on Mie theory.

3.1 Empirical formula for initial parameters

Accurate initial parameters are helpful for decreasing the computational complexity of the second step of the scheme. Frequencies of the supernumerary bows and ripple bows are both related to the droplet radius. Relationships between the radius and the

frequency are shown in Fig.6. It can be seen that the two curves are both almost linear. However, the curve corresponding to the supernumerary bows has a larger slope. As a result, the frequency offset caused by noises leads to the larger measurement error. Fig.7 illustrates the relationship between the frequency of the ripple bows and radius under different refractive indexes. It seems that the slope increases with increasing refractive index. According to the curve corresponding to the ripple bows in Fig.6, the empirical formula for the radius is obtained:

$$R = 23.89F + 1.427 \qquad (7)$$

where R is the droplet radius and F is the frequency of the ripple bows.

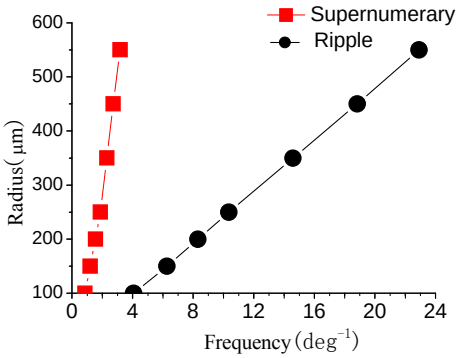

Fig.6 Frequency of the ripple bows and supernumerary bows vs. radius (m=1.3326, λ=532nm)

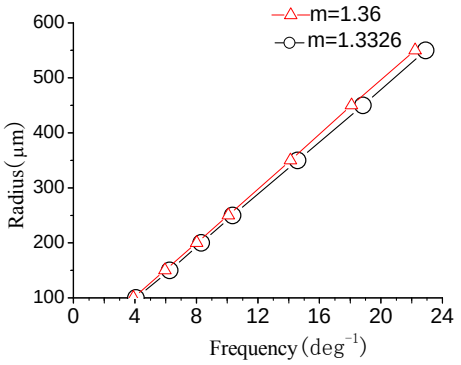

Fig.7 Frequency of the ripple bows vs. radius with different refractive index (λ=532nm)

Refractive index can be iterated with the geometrical predicted rainbow angle according to equation (2). Fig.8 illustrates the relationship between the radius and the ratio of the true refractive index to the iterative result under different refractive indexes. It can be seen that the two curves increase nonlinearly. There is a large deviation between the two curves when the radius is less than 150μm. A fourth-order correction polynomial is proposed according to the curve corresponding to m=1.3326 in Fig.8:

$$m = m_{rg} \cdot (-6.875e-13\,R^4 + 1.02e-9R^3 - 5.503e-7\,R^2 + 1.3088e-4\,R + 0.9862) \qquad (8)$$

where m is the correction value and m_{rg} is the iterative result.

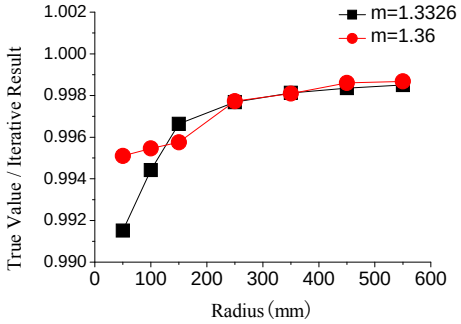

Fig.8 Ratio of the true refractive index to the iterative value vs. radius

3.2 Optimization process

The performance of the empirical formula is weak when the droplet parameters change in a broad range. Therefore the results from the empirical formula should be optimized. Fig.9 shows the values of the objective function based on Mie theory around the true parameters (m=1.333, R=80 μm). It can be seen that the function value for the true droplet parameters is minimum in the global area. However, there are many local minima around the true parameters due to the high frequency structure of the rainbow. Curve at the section of m=1.333 in Fig.9 is shown in Fig.10. It can be seen that the monotonicity of the curve is so poor that it is difficult to establish a simple optimization path. Thus the droplet parameters should be determined by optimization algorithm or ergodic process.

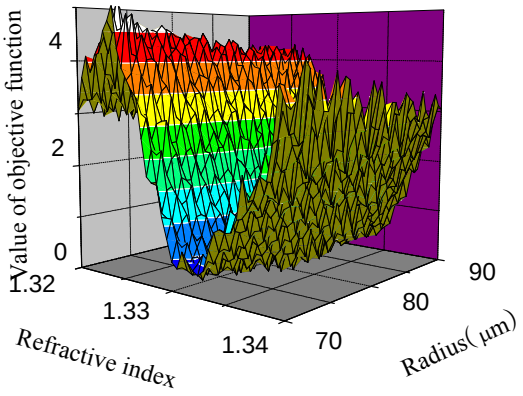

Fig.9 Values of objective function based on Mie theory (m=1.333, R=80 μm)

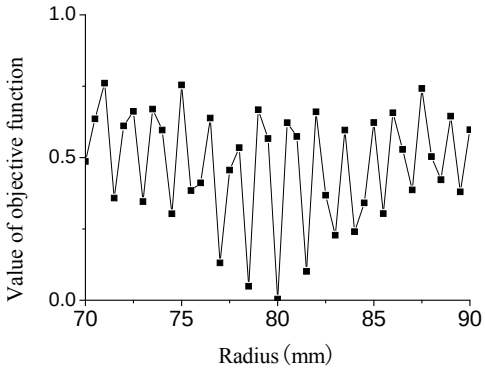

Fig.10 Relationship between function value and radius at the section of m=1.333 in Fig.9

Fig.11 illustrates the values of the objective function based on Debye theory (p=2) around the true parameters (m=1.333, R=80 μm). Curve at the section of m=1.333 in Fig.11 is shown in Fig.12 (a), and curve at the section of R=80μm in Fig.11 is shown in Fig.12 (b). It can be seen that the surface shown in Fig.11 is approximately an elliptic paraboloid. At a certain section $z=z_0$, the long axis parallel to the R-axis is far longer than the short axis parallel to the m-axis. And the surface has good monotonicity on any side of the lowest point. Thus it is helpful to estimate the optimization direction. Nevertheless, the lowest point in Fig.12 (a) does not correspond to the true parameters because of angular deviate between the low frequency component of the rainbow simulated with Mie theory and the supernumerary bows simulated with Debye theory (p=2). Therefore measurement error occurs.

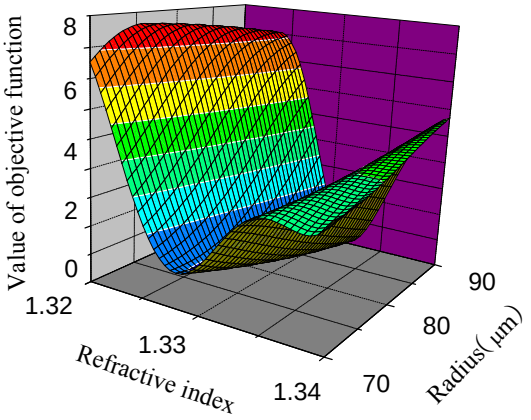

Fig.11 Values of objective function based on Debye theory (m=1.333, R=80 μm)

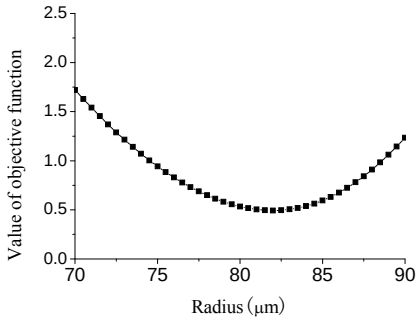

(a) The section of m=1.333

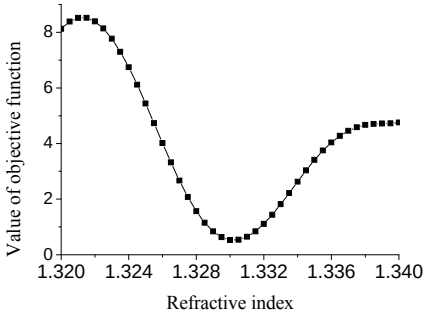

(b) The section of R=80μm

Fig.12 Two typical sections of the surface in Fig.11

Optimization process starts from the calculation results of the empirical formula (m_0, R_0). Then (m_0, R_1) is obtained by an offset to the radius R_0. Therefore the optimization direction can be estimated by comparing the objective function values of the two points. Thus optimal parameters at the section $m = m_0$ can be found. Then m_0 is adjusted with an offset. Similarly the optimal parameters at the section $m = m_1$ can be found. Finally the global optimal parameters can be found by repeating the process above.

Considering local minimum in the area of m <1.321 in Fig.12 (b), the parameter offset decreases gradually from a initial value which is large enough to ensure that optimization path can jump out of the area after entering. So the local minimum would not be selected as the global optimal points.

3.3 Further searching parameters based on Mie theory

Measurement errors exist in the optimization parameters. So they should be corrected with objective function based on Mie theory. Considering the weak regularity in Fig.9, the objective function values of several discrete points (shown as equation (9)) around the optimization one are computed in order to find the minimum corresponding to the final measurement results. It is confirmed that more discrete points means larger search range and more time-consuming. So the number of the discrete points should be designed according to the two factors above.

$$\begin{cases} m_i = m_n + 0.0002 * i, & i = -k, -k-1, \cdots, k \\ R_j = R_n + R_n \backslash 100 * j, & j = -k, -k-1, \cdots, k \end{cases} \quad (9)$$

where (m_n, R_n) is the optimization parameters of Step 2, $2k$+1 is the number of the discrete points and R_n\100 is the integer part of R_n (μm) divided by 100 (if R_n<100 then we define that R_n\100 equals 1).

4 Experimental

The nonspheric effect of free falling droplet causes large measurement error of the droplet based on rainbow technique [5]. Therefore the stable liquid column at the capillary export is achieved to avoid the nonspheric effect during the experiment in this paper, because its circle cross-section is similar to ideal sphere. Because of the viscous force between the column and the capillary, the diameter of the column below the capillary export becomes smaller when falling down, as is shown in Fig.13. Consequently liquid column 1mm below the capillary export is taken for experiment, so that the column diameter almost equals to the internal diameter of the capillary.

Fig.14 shows the schematic diagram of an experimental system, which consists of the capillary object and an optical system. Two kinds of the capillary with internal diameters of 0.5mm and 1mm are used to change the diameter of the liquid column. NaCl solution with the concentration of 0-50g/L is used to change the refractive index. The optical system consists of an optical platform, a laser (100mW, 532nm), a mirror, two convex lenses and a CCD camera (2048 pixels, 40MHz). The environment temperature is 12 □ during the experiments. The laser beam illuminates the liquid column after the mirror's reflection. Then the convex lens (1) and (2) converges the scattering light from the column onto the CCD camera. Fig.15 shows a typical first-order rainbow captured by the CCD camera. The intensity distribution corresponding to Fig.15 is illustrated in Fig.16. The abscissa in Fig.16 is the serial number of pixel, which can be transformed to the scattering angle by calibration.

Fig.13 Photo of liquid column at the capillary export

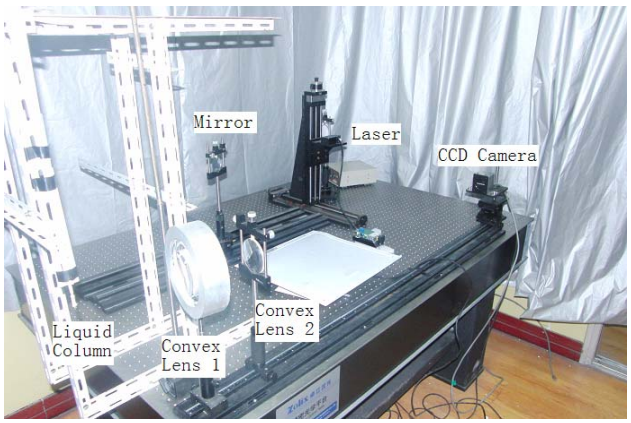

Fig.14 Experimental system

Fig.15 First-order rainbow captured by CCD camera

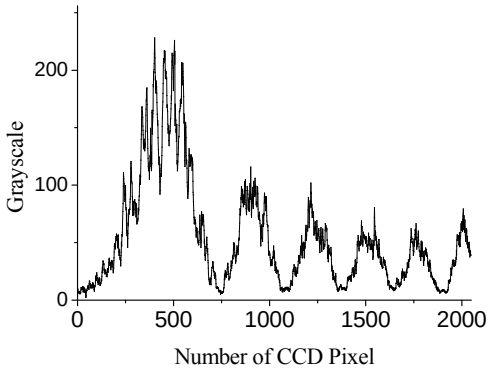

Fig.16 Rainbow intensity distribution

5 Results and discussion

According to James Hom's research in 2002, the refractive index of the pure water is 1.336 at 12□ [12]. Thus 1.336 is taken as the true the true refractive index, and the internal diameters of the capillaries are taken as the true diameters of columns. The intensity distribution of the rainbow produced by the water column at the export of 0.5 mm capillary is shown in Fig.17. The low frequency component of the detected signal and the curve simulated with Debye theory (p=2) (250μm, 1.336) are also illustrated in Fig.17. It can be seen that the angular locations of the corresponding maxima in the simulation curve and low frequency component curve are almost equal. Compared the rainbow simulated by Mie theory in Fig.4 with the captured rainbow in Fig.17, it can be seen that the ripple bows of the captured rainbow are polluted by the noises due to system vibration, pulsating flow and circuit interference. Fig.18 illustrates the frequency spectrum of the captured rainbow and the rainbow simulated by Mie theory (250μm, 1.336). It can be seen that there are several local maxima around the ripple frequency in the frequency spectrum of the captured rainbow. The rainbow produced by the water column at the export of 0.5 mm capillary is captured 10 times continuously for repeatability research. The measurement results of the refractive index are shown in Fig.19 (a), and the radius results are shown in Fig.19 (b). It can be seen that the radius results from the empirical formula have large measurement errors and the repeatability is weak. The reason is that the amplitudes of the maxima around the ripple frequency in the frequency spectrum are changed due to noises. The measurement results of the refractive index also have large errors, and the maximum error is 1.7×10^{-3}. The reason is that radius result is the variable of the empirical formula for refractive index, so the error transfer occurs. However the results of Step 2 and Step 3 have smaller errors and the respectabilities are better. The absolute errors of the refractive index results are below 5×10^{-4}, and the relative errors of the radius results are below 8%. The high accuracy of the measurement results is due to the good coincidence between the low frequency component of the captured rainbow and the simulated rainbow by Debye theory (p=2) when the true radius is big enough.

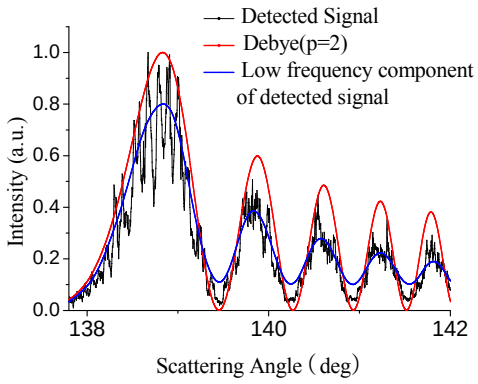

Fig.17 Low frequency component of the captured rainbow and supernumerary bows simulated by Debye theory (p=2)

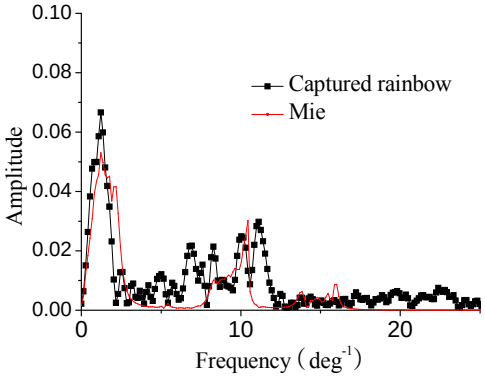

Fig.18 Frequency spectrum of the captured rainbow and the rainbow simulated by Mie theory (250μm, 1.336)

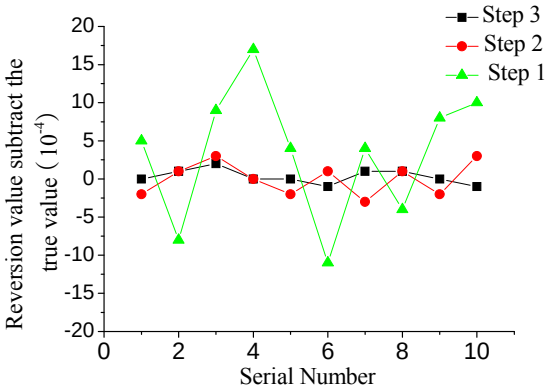

(a) Measurement errors of the refractive index results

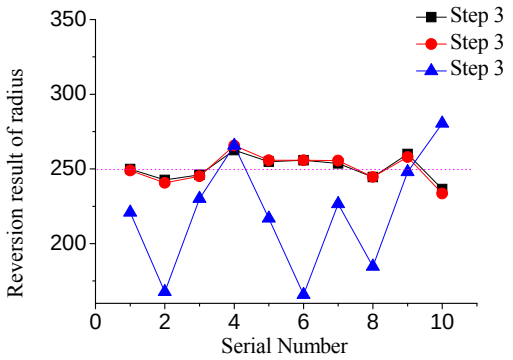

(b) Radius measurement results

Fig.19 Inversion results of the rainbow produced by water column at the export of 0.5mm capillary

Reversion parameters of the rainbow produced by NaCl solution column at the export of 0.5 mm capillary are shown in Fig.20. Fig.20 (a) illustrates the refractive index measurement results, and Fig.20 (b) illustrates the radius measurement results. Reversion results of the rainbow produced by NaCl solution column at the export of 1 mm capillary are shown in Fig.21. Fig.21 (a) illustrates the refractive index measurement results, and Fig.21 (b) illustrates the radius measurement results. The radius measurement results from empirical formula have large errors because of the noise, and the maximum relative error is 33%. While the relative errors of the radius results of Step 2 and Step 3 are below 7.5%. And the repeatability is satisfied. Compared with the refractive index measurement results of Step 1 and Step 3, the curve corresponding to Step 1 fluctuates around the curve corresponding to Step 3 in Fig.20 (a) and Fig.21 (a). The refractive index results of NaCl solution with the fixed concentration are almost equal when the diameters of the columns are different. Fig.22 shows the linear fitting curve of the mean refractive index under two column diameters. It can be seen that there is an approximately linear relationship between the refractive index and the concentration of NaCl solution. This conclusion also validates the feasibility of the concentration measurement based on rainbow refractometry.

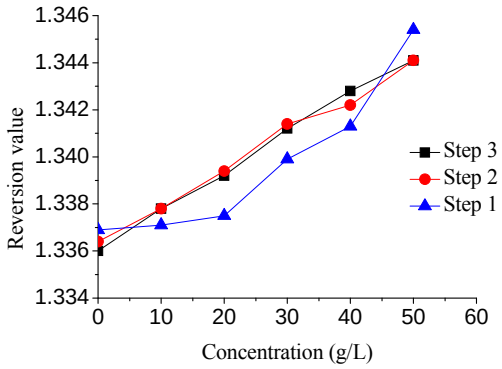

(a) Refractive index results

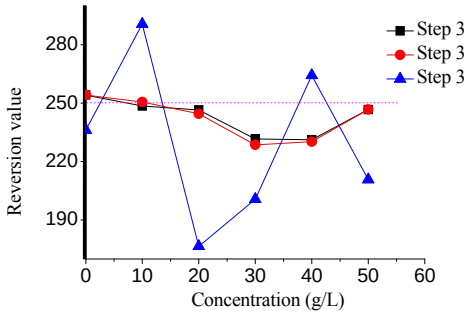

(b) Radius results

Fig.20 Inversion parameters of the rainbow produced by NaCl solution column at the export of 0.5mm

capillary

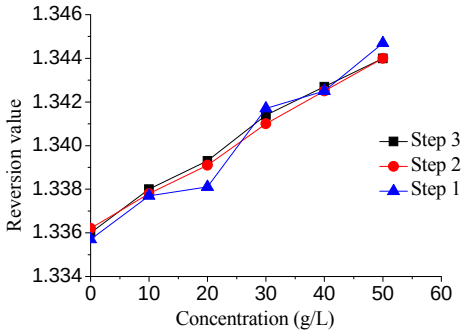

(a) Refractive index results

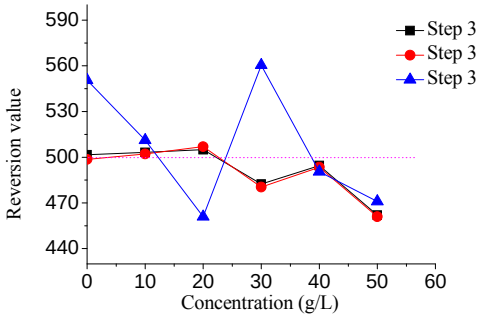

(b) Radius results

Fig.21 Inversion parameters of the rainbow produced by NaCl solution column at the export of 1mm capillary

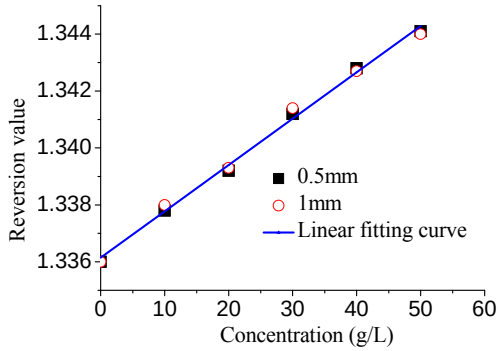

Fig.22 Linear fitting of the refractive index measurement results

The captured rainbow is polluted by the noise. Take the second supernumerary bow of the captured rainbow in Fig.17 for example, the amplitudes of the first half are bigger than those of the second half. Therefore low frequency component of the second supernumerary bow in the captured rainbow moves forward. As a result the inversion radius is bigger than the true value. If the same situation occurs in the first supernumerary bow, there would be measurement errors in both parameters. In addition, large time-consumption is the disadvantage of the scheme. The reason is that the computational complexity of Mie theory and Debye theory is proportional to the radius. When capillary with the internal diameter of 0.5mm is used, time-consumption of Step 2 is about 10s and time-consumption of Step 3 is about 15s (if the number of discrete points is 49). When capillary with the internal diameter of 1mm is used, time-consumption of Step 2 is about 28s and time-consumption of Step 3 is about 40s (if the number of discrete points is 49). It can be seen from Fig.19, Fig.20 and Fig.21 that the second step still has good performance although its accuracy is rarely lower than that of Step 3. So the third step of the scheme can be omitted to improve the real-time performance of the scheme.

6 Conclusion

An objective function is designed to quantify the deviation between the captured rainbow and the simulated rainbow, and further an inversion scheme for the radius and refractive index of a single droplet is proposed based on Debye theory (p=2) and the objective function. The experimental result shows that the relative error of the radius is better than 8%, and the absolute error of the refractive index is less than 5×10^{-4}. Compared with the method based on the empirical formula, the proposed inversion scheme has higher accuracy. Nevertheless, the inversion scheme needs large time-consumption. If the third step of the scheme is omitted to improve the real-time performance, the modified scheme still has high measurement accuracy.

Acknowledgement

The authors wish to express their gratitude to Research Award Program for Outstanding Young Teachers in Southeast University (No.3203001202) and QingLan Project (No.1103000126).

References

[1] J. Wilms and B. Weigand, Composition measurements of binary mixture droplets by rainbow refractometry, Applied Optics, 46(11), 2007: 2109-2118.

[2] N. Roth, K. Anders, and A. Frohn. Simultaneous measurement of temperature and size of droplets in the micrometer range. J Laser Appl, 1990, 2(1): 37-42.
[3] N. Roth, Klaus Anders, and Arnold Frohn. Refractive-index measurements for the correction of particle. APPLIED OPTICS, 1991, 30(33):4960-4965.
[4] N. Roth, Anders K, Frohn. Determination of size, evaporation rate and freezing of water droplets using light scattering and radiation pressure. Particle & Particle Systems Characterization, 1994, 11(3): 207–211.
[5] A J. P. A. J. van Beeck and M. L. Riethmuller. Nonintrusive measurements of temperature and size of single falling raindrops. Applied Optics, 1995(34): 1633–1639.
[6] Wu Zhensen, Guo Lixin, Han Xiang'e, Hou Shanhui. Measurement of Infinite Cylindrical Diameter by Angular Frequencies of Rainbow Intensities. ACTA OPTICAS INICA, 2000, 20(11): 1538-1543.
[7] Pan Qi. Study on non-intrusive rainbow measurement. Southeast University, Nanjing, China: 2010.
[8] H. C. van de Hulst. Light scattering by small particles. New York, U.S.A: John Wiley & Sons, 1957: 136-156.
[9] Ru T. Wang, H. C. van de Hulst. Rainbows. Mie computations and the Airy approximation. APPLIED OPTICS, 1991, 30(1): 106-117.
[10] Philip Laven. Simulation of rainbows, coronas and glories using Mie theory and the Debye series. Journal of Quantitative Spectroscopy & Radiative Transfer, 2004 (89): 257–269.
[11] Renxian Li, Xiange Han, Huifen Jiang. Debye series for light scattering by a multilayered sphere. Applied Optics, 2006,45(6):1260-1270.
[12] James Hom, Norman Chigier. Rainbow refractometry: simultaneous measurement of temperature, refractive index, and size of droplets. APPLIED OPTICS, 2002, 41(10): 1899-1907.